ELSEVIER

The Spine Journal 000 (2020) 1–10

THE SPINE JOURNAL

Basic Science

Misaligned spinal rods can induce high internal forces consistent with those observed to cause screw pullout and disc degeneration

Arjan C.Y. Loenen, MSc[a,b], David C. Noriega, MD[c], Carlos Ruiz Wills, PhD[d], Jérôme Noailly, PhD[d], Pierce D. Nunley, MD[e], Rainer Kirchner, MD[f], Keita Ito, PhD, MD[b], Bert van Rietbergen, PhD[a,b,*]

[a] *Department of Orthopaedic Surgery, Laboratory for Experimental Orthopaedics, CAPHRI, Maastricht University Medical Centre, Maastricht, the Netherlands*

[b] *Department of Biomedical Engineering, Orthopaedic Biomechanics, Eindhoven University of Technology, Eindhoven, the Netherlands*

[c] *Spine-Unit, University Hospital of Valladolid, Valladolid, Spain*

[d] *Department of Information and Communication Technologies, Barcelona Centre for New Medical Technologies (BCN MedTech), Universitat Pompeu Fabra, Barcelona, Spain*

[e] *Spine Institute of Louisiana, Shreveport, LA, USA*

[f] *Department of Orthopaedic Surgery and Trauma Surgery, Clinics Husum and Niebüll, Husum, Germany*

Received 9 June 2020; revised 31 August 2020; accepted 24 September 2020

Abstract

BACKGROUND CONTEXT: Manual contouring of spinal rods is often required intraoperatively for proper alignment of the rods within the pedicle screw heads. Residual misalignments are frequently reduced by using dedicated reduction devices. The forces exerted by these devices, however, are uncontrolled and may lead to excessive reaction forces. As a consequence, screw pullout might be provoked and surrounding tissue may experience unfavorable biomechanical loads. The corresponding loads and induced tissue deformations are however not well identified. Additionally, whether the forced reduction alters the biomechanical behavior of the lumbar spine during physiological movements postoperatively, remains unexplored.

PURPOSE: To predict whether the reduction of misaligned posterior instrumentation might result in clinical complications directly after reduction and during a subsequent physiological flexion movement.

STUDY DESIGN: Finite element analysis.

METHODS: A patient-specific, total lumbar (L1–S1) spine finite element model was available from previous research. The model consists of poro-elastic intervertebral discs with Pfirrmann grade-dependent material parameters, with linear elastic bone tissue with stiffness values related to the local bone density, and with the seven major ligaments per spinal motion segment described as nonlinear materials. Titanium instrumentation was implemented in this model to simulate a L4, L5, and S1 posterolateral fusion. Next, coronal and sagittal misalignments of 6 mm each were introduced between the rod and the screw head at L4. These misalignments were computationally reduced and a physiological flexion movement of 15° was prescribed. Non-instrumented and well-aligned instrumented models were used as control groups.

RESULTS: Pulling forces up to 1.0 kN were required to correct the induced misalignments of 6 mm. These forces affected the posture of the total lumbar spine, as motion segments were predicted to rotate up to 3 degrees and rotations propagated proximally to and even affect the L1–2 level.

FDA device/drug status: Not applicable.

Author disclosures: ***ACYL***: Research Support (Investigator Salary, Staff/Materials): 4WEB Medical (Paid as salary). ***DCN***: Consulting: Vexim-Stryker (C). ***CRW***: Nothing to disclose. ***JN***: Fellowship Support: Spanish Government (A). ***PDN***: Nothing to disclose. ***RK***: Nothing to disclose. ***KI***: Board of Directors: AO Foundation (D); Scientific Advisory Board/Other Office: NC Biomatrix BV (B). ***BvR***: Grant: Neomedical (D).

*Corresponding author. Department of Biomedical Engineering, Eindhoven University of Technology, Building 15, Gemini-Zuid (4.118), P.O. Box 513, 5600 MB Eindhoven, the Netherlands, Groene Loper, TU Eindhoven, De Rondom 70, 5612AP Eindhoven, the Netherlands. Tel.: +31 40 247 4350.

E-mail address: b.v.rietbergen@tue.nl (B. van Rietbergen).

https://doi.org/10.1016/j.spinee.2020.09.010

The facet contact pressures in the corrected misaligned models were asymmetrical suggesting non-physiological joint loading in the misaligned models. In addition, the discs and vertebrae experienced abnormally high forces as a result of the correction procedure. These effects were more pronounced after a 15° flexion movement following forced reduction.

CONCLUSIONS: The results of this study indicate that the correction of misaligned posterior instrumentation can result in high forces at the screws consistent with those reported to cause screw pullout, and may cause high-tissue strains in adjacent and downstream spinal segments.

CLINICAL SIGNIFICANCE: Proper alignment of spinal posterior instrumentation may reduce clinical complications secondary to unfavorable biomechanics.

Keywords: Finite element analysis; Pedicle screw; Rod contouring; Spine biomechanics; Spinal fusion

Introduction

Pedicle screw and rod constructs are commonly used to provide posterior spine stabilization in a wide variety of spinal disorders [1]. Such constructs can involve the fixation of one spinal motion segment or more. With more segments involved, manual contouring of the spinal rod is commonly necessary to obtain proper alignment of the screw heads and the rod [2]. However, residual mismatches are expected, even after contouring [3]. The relevance of such mismatches has long been dismissed as dedicated reduction devices are typically available to assist the surgeon in assembling the construct. These devices mechanically force the spinal rod into the head of the screw but do not control the exerted forces, which may lead to excessive reaction forces that may result in clinical complications [4].

Previous ex vivo biomechanical research revealed that the correction of clinically relevant residual mismatches by a reduction device may decrease screw pullout strength, or even provoke instantaneous screw pullout [5−7]. Even if screw pullout does not occur, it is possible that the reduction of residual mismatches can have undesirable effects, that is, increased facet joint and intravertebra forces, and increased intervertebral disc deformations [8]. The corresponding mechanical loads and induced tissue deformations are however not well identified. Additionally, whether the forced correction of the mismatch alters the mechanical behavior of the lumbar spine during postoperative physiological movements is unexplored.

Finite element (FE) analysis of the spine enables quantification of biomechanical parameters impossible to acquire experimentally, allows for multistep procedures, and has previously been acknowledged as valuable tool to address clinically relevant problems [9,10]. Therefore, we used FE analysis in this study to reveal both the direct and the indirect consequences of the correction of the mismatch. Using this approach, a posterolaterally fused lumbar spine was modeled, introducing perfectly fitting rods or clinically relevant mismatches. The first aim was to analyze the mechanical loads and deformations both in the instrumentation and surrounding tissue when performing the mismatch correction procedure. The second aim was to analyze the biomechanical loads in the corrected, posterolaterally fused, lumbar spine during a physiological flexion movement. Two different scenarios were employed by inducing a mismatch between rod and screw head, in the coronal and in the sagittal plane, respectively. Finally, the presence of a fixed contralateral construct was varied to evaluate the impact of different surgical situations.

Methods

FE models of the intact lumbar spine

An FE model that includes the vertebrae L1−L5 and the discs L1−2 to L5−S1 was used in this study. It originated from the EU-funded MySpine project (EU FP7-ICT 269909) that included lower back pain patients and was approved by the Scientific Research Ethics Committee of the Medical Research Council (751/PI/2010) of the National Center for Spinal Disorders, Budapest, Hungary. Details of the patients and models can be found elsewhere and are only summarized here [11,12]. Computed tomography (CT) and magnetic resonance imaging (MRI) scans were used to segment the vertebrae and intervertebral discs (IVDs), respectively [13,14]. MRI scans enabled identification of the nucleus pulposus (NP) and annulus fibrosis (AF) regions of each IVD. Both segmentations were performed with a trained algorithm following the active shape modeling framework as introduced by Cootes et al. [15]. The mesh of a generic FE model was morphed to the patient, based on anatomical landmarks as described in Castro-Mateos et al. [16]. The model used in this study was based on data of a 55-year-old female patient with a weight of 74 kg, height of 167 cm, and Pfirrmann grades of III, III, III, IV, and III for disc L1−2 to L5−S1. This patient was selected from the database since she represented a typical patient case of the degenerative spine eligible for spinal fusion surgery [17].

The bony posterior elements, facets, and bony endplates were modeled as isotropic linear elastic materials. For the vertebral bodies, patient-specific trabecular bone densities were integrated in the model by relating the transversely isotropic, linear elastic material properties of the elements

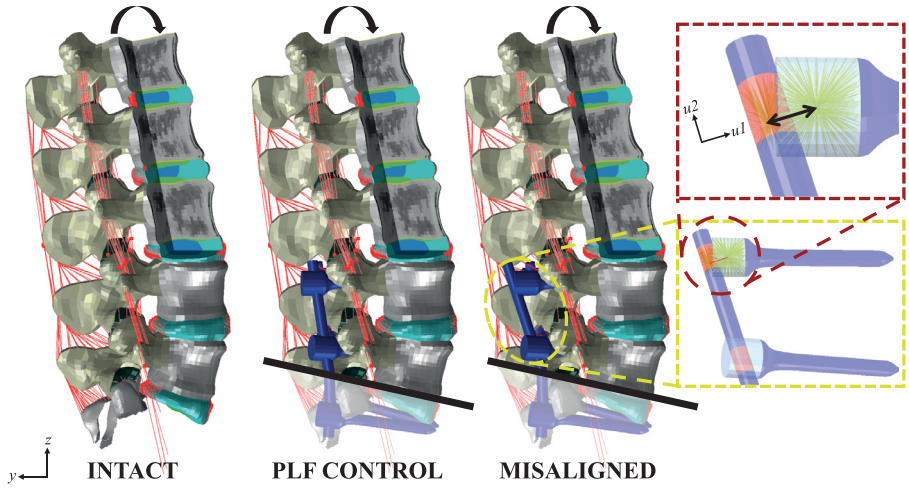

Fig. 1. Overview of the intact control, posterolaterally fused control, and sagittally misaligned model. Different colors represent different material properties for ligaments, bony posterior ends, facets, sacrum, cortical bone, trabecular bone with density-dependent stiffness, annulus fibrosis, nucleus pulposus, cartilage endplates, bony endplates, and titanium. On the right, the element set (in red) that is required to be located in the screw head (lucent blue). A connector element (black double arrow) was defined between the central point of the rod and screw head elements respectively. U is the local coordinate system of the connector element with u1 along the direction of the connector element and u2 along the longitudinal axis of the spinal rod.

to the mean CT gray value calculated within the representative volume of each element [18]. The sacrum and cortical bone were modeled as orthotropic linear elastic. Facet joint articulation was modeled by surface-to-surface frictionless contact resolved through a penalty algorithm with a penalty normal stiffness of 200 N/mm [19]. The cartilage endplates were modeled as isotropic poro-elastic [20]. The NP and AF were both modeled by a poro-hyperelastic material model, assuming a Neo-Hookean material to determine the strain energy density for the isotropic solid matrix. For the AF, an additional anisotropic term was added to the strain energy density function representing the contribution of the cross-ply collagen fibers during positive strain of the AF [21]. The total stress resulting from the external load was defined as the superposition of the porous solid stress and the fluid pore pressure. The strain energy density function and Darcy's law were used to derive the porous solid stress and fluid pore pressure, respectively. For the NP, a swelling pressure-related term was introduced in order to describe proteoglycan-induced NP swelling [11]. For each poro-(hyper)elastic material model, a strain-dependent permeability was included and updated during the simulations. All IVDs were previously graded by an experienced radiologist based on the Pfirrmann classification [22]. Depending on the Pfirrmann grade, different material parameters were adjusted for the NP and AF based on Malandrino et al. [11]. Ligaments were included in the model and described as hypoelastic unidirectional materials. The stress-strain relationship was described by an initial nonlinear toe region, modeled by a fitted power law, followed by a simple linear function. Fiber stiffness parameters were defined per ligament type and disc level [23], and were further optimized to reproduce the ex vivo experimental data of full L1–S1 specimens from Malandrino et al. [11].

The FE model as described above is referred to as the control or intact model (Fig. 1). The calculation outputs of this model served as reference values for the physiological flexion movement analysis. The simulations started with a pre-conditioning step of 8 hours that allowed for pre-swelling of the poro-(hyper)elastic IVDs. During this initial step, the caudal end of the spine was completely constrained while the cranial end was allowed to translate as consequence of changing disc height. Subsequently, a flexion rotation of 15° applied in 5 seconds was prescribed as physiological movement of the lumbar spine.

FE model of the posterolaterally fused lumbar spine

Titanium (Ti-6Al-4V) pedicle screw and rod instrumentation was implemented into the intact model based on anatomical landmarks. Polyaxial screw heads without any rotational restrictions were assumed in the model. In this study, an L4–S1 bisegmental posterolateral fusion was simulated assuming L5–S1 instrumentation was already tightened. This assumption allows for replacement of the disc of segment L5–S1 and its corresponding posterior instrumentation by constraining boundary conditions. Each screw was fixed in the corresponding vertebra by embedding constraints. The titanium rods could be embedded in the screw heads under every angle provided that previously specified caudal and cranial element areas were located within the screw head. In this way, polyaxial screw heads could be modeled without requiring geometrical rearrangement of the mesh of the screw heads (Fig. 1).

This model represents an L4–S1 posterolateral fusion without any mismatch between screw heads and fixation rod (well-aligned posterolateral fusion control [PLF] control). Similar to the non-instrumented control model, this

model starts with a pre-conditioning period of 8 hours. The posterior instrumentation was implemented right after the pre-conditioning step, just before the flexion rotation of 15 degrees was prescribed. The output data of this model provided reference values for the physiological flexion movement of a well-instrumented posterolaterally fused (L4−S1) spine.

FE model of the misaligned posterolateral instrumentation in the lumbar spine

The PLF control model was altered to induce a misalignment of 6 mm between the right rod and the right screw head of L4. The orientation of the rod was manipulated such that a misfit was introduced in either the coronal or sagittal plane while retaining the fit between the right rod and the screw head of L5. For the coronal respectively sagittal misalignment, the rod was positioned 6 mm medially and posteriorly with respect to the right screw head of L4. The nodes constituting the head of the right screw of L4 were all rigidly coupled to their central location. Also the nodes in the region of the rod that is designated for fixation in the screw head (depicted in red in Fig. 1) were all coupled to their central location. Then, a 3D connector element that can be reduced in length was implemented between these two points. The direction of this connector element was used to specify the pulling (reduction) direction, that is, mediolateral and anteroposterior for the coronal and sagittal misalignment, respectively (u1-axis in Fig. 1). During pulling, movement along the longitudinal axis of the spinal rod was allowed (u2-axis in Fig. 1).

Again, the model starts with an initial pre-conditioning period of 8 hours without instrumentation being present. After the pre-conditioning step, the misaligned posterior instrumentation was implemented and a 5-second correction procedure was simulated by contraction of the connector element while vertebra L1 was constrained at its post-swelling position. For both misaligned configurations, two different surgical situations considering the presence of a contralateral construct at segment L4−5 were analyzed. Situation I assumed that the contralateral side, on the left, was fixed without misalignment prior to the correction procedure. On the contrary, situation II assumed that the contralateral side was not stabilized yet during the correction procedure. Following the correction, the rod and screw head on the right were fastened and a well-aligned contralateral rod was introduced and fastened on the left. Then, the flexion rotation of 15° was prescribed.

Output analysis

The FE solver ABAQUS/Standard (Simulia, Inc., Providence, RI) version 2018 was used for solving the described models. The force that was required for pulling rod and screw toward each other was determined post-correction. In addition, the relative rotation for each of the vertebrae was calculated post-correction and post-flexion. A Matlab script, based on Horn's quaternion-based method [24], was used to determine the rotation matrix that best maps the original position of the nodes of the vertebra's corpus on their updated position after correction and flexion respectively. For each vertebra, the rotation matrix relative to its caudal neighbor was derived as described by Kingma et al. [25]. Then, the relative rotation matrix was decomposed using Tait-Bryan chained rotations. The adopted order of axis was horizontal, anteroposterior, and longitudinal axis providing angular motions in the sagittal, coronal, and axial plane, respectively. Also, the maximum contact pressures per facet joint were estimated post-correction and post-flexion. Besides, the reaction moment at the cranial end of vertebra L1 was monitored after realizing the flexion movement. Both post-correction and post-flexion, the volume of tissue that is at risk for damage was quantified in the bony structures and IVDs. A bone element was considered vulnerable for local damage when its absolute maximum principal strain value exceeded 1% [26]. For IVD elements, a threshold value of 20% major principal strain was considered to promote biological responses associated with disc degeneration [27].

Results

Post-correction analysis

The pulling forces required to reduce the rod completely into the screw head were 0.9 and 1.0 kN for the coronal and sagittal misalignment, respectively, assuming the contralateral side was already rigidly fixed (situation I). When the contralateral side was not fixed yet (situation II), the required pulling forces decreased to 0.7 kN for the correction of both the coronal and sagittal misalignments.

The induced angular motions of the functional spinal units (FSUs) were predominantly in the plane in which the misalignment was initially introduced. Rotations were smaller when the contralateral rod was already tightly fixed during the correction. FSUs L2−3 and L3−4 consistently showed opposite rotations compared to L1−2 and L4−5. Overall, rotations up to 3 degrees were induced during correction (Fig. 2).

Table 1 gives an overview of the maximum contact pressure in the facet joints for the different models. Especially for the coronal misalignment, the maximum facet pressure was 40% to 180% larger when the contralateral rod was not implemented yet (situation II). Asymmetrical increased facet contact pressures of up to 6 MPa were found cranial to L4−5 after correction of the misalignment.

The tissue volumes at risk after the correction procedure are presented in Table 2. In general, the correction of the coronal misalignment induced larger tissue volumes at risk in the bone, whereas the correction of the sagittal misalignment induced larger tissue volumes at risk in the IVDs. Having the contralateral rod already rigidly fixed (situation I) generated higher tissue volumes at risk in the bone and

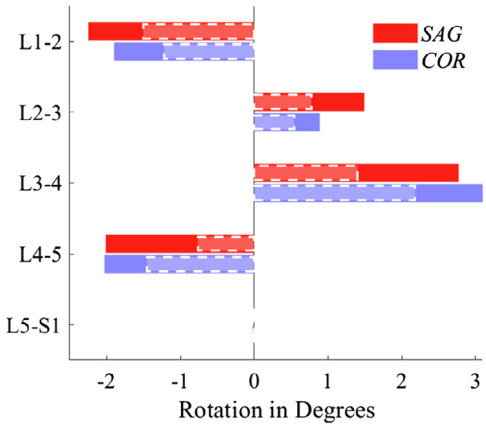

Fig. 2. Main angular motion per FSU after correction of the misalignment. For both misalignments, the main angular motion was found in its corresponding anatomical plane. Therefore, values represent rotation in the coronal (blue) and sagittal (red) plane as result of correcting the coronal and sagittal misalignment respectively. Negative/positive rotation means left/right bending in the coronal plane and extension/flexion in the sagittal plane. Dashed insets: situation I. Solid bars: situation II.

lower tissue volumes at risk in the IVD compared to the situation in which the correction was performed while the contralateral rod was not fixed (situation II).

Post-flexion analysis

For the intact control spine, the angular motion in the sagittal plane was on average 3 degrees for each of the 5 FSUs. For the PLF control and misaligned models, the rotation in the sagittal plane increased up to 6 degrees at L1–2, L2–3, and L3–4, while the rotations decreased down to zero degrees at the fixed discs L4–5 and L5–S1.

The maximum contact pressure in the facet joints in the corrected misaligned models generally decreased as result of the flexion movement (data not shown). The reaction moment in a 15-degree flexion configuration was 8 Nm for the intact control spine. The instrumented spine models required significantly higher moments to achieve this configuration: 26, 22, 23, 31, and 37 Nm for PLF control, coronal misalignment situations I, II, and sagittal misalignment situations I, II, respectively.

The tissue volumes at risk after having simulated the flexion movement are summarized for the different models in Table 2 and graphically displayed in Fig. 3. Comparing the post-flexion with the post-correction values for the misaligned situations, the tissue volume being at risk increased within the IVDs. Additionally, new bone tissue volume at risk was introduced as consequence of the flexion movement. The PLF control model shows the same trends while the intact control model shows only IVD tissue at risk during the physiological flexion movement.

Discussion

The purpose of this study was to predict the loads and deformations associated with the correction of a misalignment between the spinal rod and the pedicle screw heads,

Table 1.
The maximum facet contact pressure [MPa] found at the left and right joint after performing the correction procedure for the coronal (COR) and sagittal (SAG) misalignment in situations I and II, respectively

	$L1-2_{left}$	$L1-2_{right}$	$L2-3_{left}$	$L2-3_{right}$	$L3-4_{left}$	$L3-4_{right}$	$L4-5_{left}$	$L4-5_{right}$
COR I	-	4.0	-	2.8	-	3.9	3.2	-
COR II	-	6.3	-	3.9	-	5.1	9.0	-
SAG I	-	2.0	-	2.1	-	3.3	-	-
SAG II	-	1.3	-	1.0	0.6	4.1	-	-

Table 2.
Tissue volume at risk in the vertebrae and intervertebral discs [mm^3] for the misaligned and control models after simulation of the correction and the flexion motion. Post-correction and post-flexion values are shown for the coronal (COR) and sagittal (SAG) with (I) and without (II) having fixed the contralateral rod before the correction. Additionally, the results for the intact and well-aligned posterolateral fusion control (PLF) are shown.

		Vertebrae					Intervertebral discs				
		L1	L2	L3	L4	L5	L1–2	L2–3	L3–4	L4–5	L5–S1
Post-correction	COR I	-	-	-	45	-	-	-	6	14	n/a
	COR II	-	-	-	22	-	13	-	152	62	n/a
	SAG I	-	-	-	1	12	115	1	76	3490	n/a
	SAG II	-	-	-	-	3	164	40	269	3869	n/a
Post-flexion	INTACT	-	-	-	-	-	2	30	10	2	165
	PLF	10	2	1	2	-	1424	1227	1888	327	n/a
	COR I	16	1	-	60	-	1096	926	1596	371	n/a
	COR II	23	1	-	30	-	1263	1087	1748	810	n/a
	SAG I	33	3	1	2	18	1875	1823	2399	4148	n/a
	SAG II	47	5	1	6	3	2396	2372	2994	5078	n/a

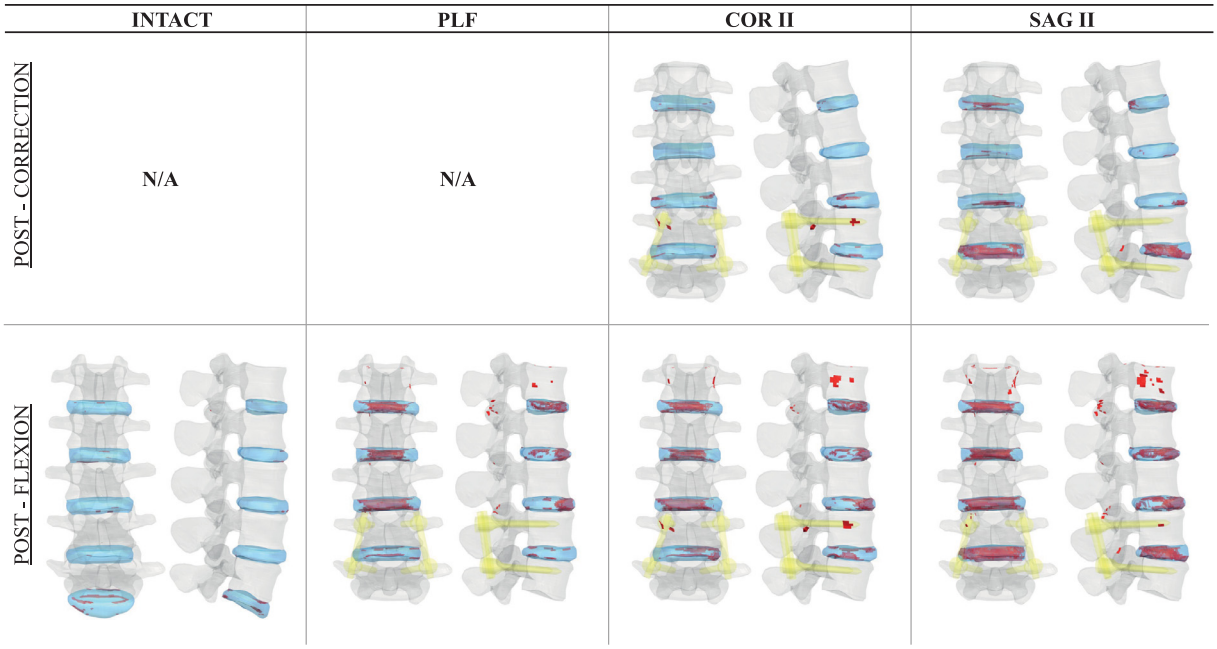

Fig. 3. Graphical representation indicating the tissue volumes being at risk after correction and flexion (gray: vertebrae, blue: IVDs, yellow: instrumentation, red: tissue at risk). The intact control showed hardly any tissue being at risk while the well-aligned posterolaterally fused control shows substantial volume at risk post-flexion. Correcting the coronal (COR) and sagittal (SAG) misalignment in which the contralateral rod was not implemented yet during correction (situation II) showed to induce adverse tissue deformations. These volumes increase during flexion following the correction procedure.

directly after having simulated the operation and a subsequent postoperative physiological flexion movement. Results demonstrate that the correction of small (6 mm) residual mismatches between spinal rod and pedicle screw head may induce forces and deformations that potentially lead to clinical complications.

Independent of the direction of misalignment and presence of the contralateral rod, excessive forces (0.7−1.0 kN) were required to correct a small misalignment of 6 mm. Lumbar pedicle screw pullout has been reported to occur at mean forces of 0.3 to 1.4 kN [28−30], depending on bone mineral density, screw type, use of cement, and insertion torque. Our results indicate, therefore, that there might be a considerable risk for screw pullout intraoperatively or postoperatively because of misalignment. For the correction of the sagittal misalignment, a direct comparison between reported pullout forces and predicted pulling forces is relevant as the applied force during rod-screw reduction was mainly oriented along the longitudinal axis of the pedicle screw. For the correction of the coronal misalignment, predicted force values are, however, not directly comparable to reported pullout forces, since the force exerted during correction was oriented perpendicular to the longitudinal screw axis. In order to preclude these excessive forces from being applied, it would be recommended to implement an overload protection for reduction devices utilized in surgery.

The excessive correction forces were found to affect the posture of the total lumbar spine as motion segments were observed to rotate and rotations propagated up to L1−2 included. Compared to a rotation per FSU of 1 to 10 degrees during different physiological movements of the lumbar spine [31], the extra rotations induced by the correction only (up to 3 degrees) are considered substantial. It is hypothesized that these additional segmental rotations may induce clinical implications on the longer term as segmental imbalances will chronically change the local load distribution and increase the risk for developing not only adjacent segment disease [32,33] but also downstream segment disease, that is, the onset of tissue deterioration at multiple levels distance of the operated segments. Segment L2−3 and L3−4 were oppositely angulated to L4−5 to compensate for the induced movement at the level of misalignment. This was due to the assumption that the cranial end of L1 was completely constrained at its post-swelling position, to ensure normal posture. Although some rotation at the T12−L1 level may occur in reality, thus leading to slightly different spinal deformation curves, this is not expected to affect the main results with regard to the forces in the lumbar spine.

The maximum facet joint contact pressure at L4−5 strongly increased on the left side during correction of the coronal misalignment, which occurred because the misalignment was introduced by placing the rod medially with respect to the upper right screw in L4. Consequently, L4 should translate toward the left, generating a movement analog to a left lateral bending in order to correct the misalignment. Following this movement, the right facet joint will open while the left one will close. Because of the opposite angulation at higher levels, increased pressures were

found on the right side in facet joints cranial to L4–5. As for correction of sagittal misalignment, there was no increase in maximum facet contact pressure at L4–5. Since an extension rotation of L4–5 was induced during correction, the decreasing lumbar lordosis angle closed mainly the right fact joints (since the correction was also applied on the right). In general, the maximum facet contact pressures cranial to the corrected segment range up to 6 MPa. Because compressive load of the spine was not modeled and lumbar facet joints open in a flexed posture [34], the intact models did not provide reference values for physiological facet contact pressures to which the values in the other situations could be compared. Consulting previous literature, El-Bohy et al. reveal physiological facet contact pressures of 0.1 to 0.3 MPa under body weight combined with a 15 Nm flexion moment in their ex vivo experiments [35]. Additionally, Du et al. predict mean and maximum facet contact pressures up to 5 and 9 MPa respectively in their in silico approach considering every basic spine movement under ±7.5 Nm, combined with a follower preload varying from 0 to 1200 N [36]. Comparing these values with the predicted maximum facet contact pressures in this research, it can be concluded that the deformations, induced by correction of the misalignment, cause relatively large, asymmetric facet joint pressures in the joints adjacent to the initially misaligned segment. Although there is no particular damage threshold for facet pressure, overloading is generally suggested to accelerate degeneration of the joint [37].

Correction of a 6 mm misalignment made the bone and IVD tissues to be at risk of damage. To correct the coronal misalignment, a medial-lateral repositioning is required. As consequence, the closing facet joints on one side restrict further segmental movement. Hence, the correction of the coronal misalignment results mainly in overloaded bone tissue. The amount of IVD tissue being at risk after correction of the coronal misalignment seems to be limited. It should however be emphasized that the IVD tissue will experience the induced deformation uninterruptedly as the spine is fixed in this deformed configuration. While appropriate dynamic loading of the IVD promotes the anabolic response of the disc, static loading favors the catabolic response suggesting a negative impact of these deformations on the longer term [38]. Besides, due to slow turnover of the IVD [39], possible disturbance of the natural balance of matrix synthesis and degradation may be clinically expressed long after surgery. The correction of the sagittal misalignment requires an anterior-posterior repositioning, which the anatomical configuration of the facet joints allows through an extension rotation of the FSU. As a result, deformations are mainly induced in the IVD instead of in the bony structures. The correction of the sagittal misalignment thus mainly translates into tissue volume at risk within the IVD. Obviously, many combined misalignments of various magnitudes can exist, for example, a screw head that is misaligned both anteroposteriorly and mediolaterally. Investigating such combinations was outside the scope of this publication, but potentially could introduce even higher forces and deformations with downstream deleterious consequences.

The presence of the contralateral rod during correction had a significant influence on the consequences of the correction procedure. Generally, the situation in which the rod was already tightened (situation I) allowed less segmental motion since the segment is partly immobilized before performing the correction procedure. Therefore, higher pulling forces were required while the induced segmental rotations were smaller. This caused higher internal stresses in the bone, generating more bone tissue volume being at risk. Additionally, higher pulling forces increase the risk for intraoperative screw pullout undoubtedly. In contrast, situation II resulted in slightly higher contact pressures in the facet joints and more IVD tissue volume being at risk because of the larger segmental motions induced by the correction. It should be noted that with a circumferential fusion operation, the disc is removed and replaced by an interbody fusion cage, and the increased loading calculated here for the disc may not be representative for the loading the cage is subjected to. An extension of the model with a cage would be needed to investigate if similar conclusions hold in case of using interbody fusion cages.

In a flexion posture of 15 degrees, the intact control model shows no bone tissue at risk but does show a relatively small volume of IVD tissue at risk. This might indicate that the damage threshold for the IVD tissue was chosen somewhat too low. However, most of this volume was found at the edge of the IVD suggesting this could also result from mesh imperfections secondary to morphing the generic FE mesh on the patient-specific geometry without additional re-meshing [40]. Nevertheless, all the instrumented models show substantially more bone and IVD tissue being at risk compared to the intact control model. This originates from the fact that segments L5–S1 and L4–5 are stabilized with posterior instrumentation. As a consequence, the other segments will be more severely deformed in order to allow the spine model to meet the prescribed flexion movement. The adjacent segments are thus at increased risk for degeneration, a phenomenon known as adjacent segment disease [41–43]. For the corrected coronal misaligned spine in flexion, there are minor differences with respect to the well-aligned instrumented spine in flexion as the correction of the coronal misalignment had little influence on the sagittal posture of the spine. The IVD volume at risk is slightly lower while the bone volume at risk is higher in the corrected coronal misaligned spine in flexion. Moreover, the large bone volume at risk as result from the correction procedure remains present in vertebra L4 during flexion. Compared to the well-aligned instrumented spine in flexion, the corrected sagittal misaligned spine showed a larger amount of bone and IVD tissue being at risk in flexion. This can be explained by the fact that the misalignment was introduced by misaligning the rod posteriorly with respect to the upper right screw of L4. As a

consequence, the correction procedure induced an extension movement of segment L4–5 before the flexion movement was prescribed, explaining a larger moment and tissue volume at risk in the subsequent flexion than in the other instrumented cases. This is consistent with previous literature that reveals sagittal imbalance as one of the risk factors for developing degeneration at levels adjacent to the fused segment [43,44]. In agreement with clinical observations, this phenomenon is in all models most expressed in the segment immediately adjacent to the fusion, that is, segment L3–4. Interestingly, the bone tissue at risk is high for L1 during flexion in all but the intact model. It should be noted, however, that the calculated risk depends on several factors, including the size and anatomical shape of the vertebrae, the load distribution between facet joints and discs, and the bone density distribution, and thus can be different for different patients.

The influence of the presence of the contralateral rod could be clearly observed in the post-correction configuration. These effects continue to exist in the flexion posture at the operated FSU, that is, in presence of the contralateral rod (situation I) more bone tissue is at risk than in absence of the contralateral rod (situation II) at L4–5. Additionally, it was rationalized that situation II allowed for larger segmental motions during the correction procedure affecting the natural posture of the spine more rigorously. As a consequence, larger tissue deformations are subsequently found for all the discs and the vertebrae proximal to the operated FSU in situation II when prescribing 15 degrees flexion without allowing any off-plane rotations. In general, the maximum contact pressures in the facet joints decrease in all models in flexion posture since the contact layers are moving away from each other during forward bending.

Although the presented FE models analyzed the biomechanical consequences of screw-rod reduction quantitatively, output data should be carefully interpreted. For example, the adopted thresholds for considering bone respectively IVD tissue being at risk follow different principles. On the one hand, the bone damage threshold predicts a direct initiation of local damage, clinically presented as immediate posterior pain due to trabecular damage. On the other hand, the adopted threshold for IVD tissue is expected to induce effects on the longer term when being experienced cyclically, clinically presented as the development of degeneration. Although it is premature to interpret the exact quantity of the tissue volume at risk, the relative changes between different situations and load-steps indicate a relative risk of that particular configuration. To get a more extensive validation of the tissue being at risk, we need to implement nonlinear material behavior for the bone, including elastic-plastic-damage behavior, and to implement a tissue degeneration model for the disc [12]. This would involve the introduction of many new parameters and require further experimental validation of the model which is outside the scope of this publication.

Limitations of the current models can be found in several assumptions that were made. First, as explained before, it is assumed that the cranial end of L1 is unaltered by the correction procedure. This was assumed since it is known that patients will try to retain their original upright posture postoperatively but it is possible as well that part of this adaptation is in the thoracic spine. Second, the replacement of posteriorly fixed segment L5–S1 by constraining the caudal end of L5 might have resulted in overestimation of the correction effects. Since the segment was only posteriorly fixed, limited motion of the FSU might be expected [45,46]. This may explain the relatively high moments that were found for the instrumented cases. Third, plasticity was not included in the material model of the titanium instrumentation. Since the von Mises stress of some of the elements in the right rod exceeded the yield stress during correction, plastic deformation will be expected, leading to lower forces than predicted here. Fourth, only one specific patient was analyzed in this research. Nevertheless, the same reduction is expected to generate similar forces in other patients, as long as rods and vertebrae are similar in size. The predicted bone tissue volume at risk, on the other hand, will also depend on the bone density distribution since the tissue at risk is based on a strain limit. Finally, our results are valid only for the situation during and directly after the surgery. After progression of bony fusion, the loads on the instrumentation as well as on the adjacent levels may change.

Because both sagittal and coronal misalignment, as well as different clinical situations considering the presence of the contralateral rod were established, only one basic spine movement was modeled in this study. It may be appreciated that the exact output depends on both the direction and size of the misalignment, and the direction and size of the considered movement. Therefore, it is recommended to include several phenotypes of misalignments and different physiological movements in future work in order to analyze the consequences of the correction procedure in greater detail. Additionally, the induced misalignment of 6 mm was chosen based on the rod size and recommendation from clinicians, who indicated that deviations in the order of the diameter of the rod were realistic to occur. This value complies with other values tested in ex vivo experiments [5]. Moreover, it is expected that this deviation between rod and screw head will only increase when the amount of included spinal segments increases.

In conclusion, the FE analysis in this study demonstrates the importance to minimize the residual mismatch between spinal rod and pedicle screw head during posterolateral fusion surgery in the lumbar spine. Avoiding the need for reduction procedures may reduce the loads both on the posterior construct and on adjacent hard and soft tissues. We postulate that clinical complications secondary to unfavorable biomechanics could be reduced by ensuring proper screw rod construct alignment such that minimal external and unintended forces

are required for connecting the spinal rods to the heads of the pedicle screws.

Acknowledgments

This study was financially supported by Neo Medical.

References

[1] Haschtmann D, Ferguson SJ. Spinal instrumentation. In: Boos N, Aebi M, editors. Spinal disorders: Fundamentals of diagnosis and treatment. Berlin, Heidelberg: Springer; 2008. p. 67–90.

[2] Wanivenhaus F, Neuhaus C, Liebmann F, Roner S, Spirig JM, Farshad M. Augmented reality-assisted rod bending in spinal surgery. Spine J 2019;19(10):1687–9.

[3] Fiere V, Armoiry X, Vital JM, Lafage V, Berthiller J, Barrey C. Preoperative planning and patient-specific rods for surgical treatment of thoracolumbar sagittal imbalance. In: van de Kelft E, editor. Surgery of the spine and spinal cord: a neurosurgical approach. Cham: Springer International Publishing; 2016. p. 645–62.

[4] Tohmeh A, Isaacs RE, Dooley ZA, Turner AW. Long construct pedicle screw reduction and residual forces are decreased using a computer-assisted spinal rod bending system. Spine J 2014;14(11):S143–S4.

[5] Paik H, Kang DG, Lehman Jr. RA, Gaume RE, Ambati DV, Dmitriev AE. The biomechanical consequences of rod reduction on pedicle screws: should it be avoided? Spine J 2013;13(11):1617–26.

[6] Kang DG, Lehman Jr. RA, Wagner SC, Bevevino AJ, Tracey RW, Gaume RE, et al. Effects of rod reduction on pedicle screw fixation strength in the setting of Ponte osteotomies. Spine J 2015;15(1):146–52.

[7] Ohba T, Ebata S, Oba H, Koyama K, Haro H. Risk factors for clinically relevant loosening of percutaneous pedicle screws. Spine Surg Relat Res 2018;3(1):79–85.

[8] Umehara S, Zindrick MR, Patwardhan AG, Havey RM, Vrbos LA, Knight GW, et al. The biomechanical effect of postoperative hypolordosis in instrumented lumbar fusion on instrumented and adjacent spinal segments. Spine 2000;25(13):1617–24.

[9] Fagan MJ, Julian S, Mohsen AM. Finite element analysis in spine research. Proc Inst Mech Eng 2002;216(5):281–98.

[10] Noailly J, Lacroix D. 5 - Finite element modelling of the spine. In: Ambrosio L, Tanner E, editors. Biomaterials for spinal surgery. Woodhead Publishing; 2012.. 144-234e.

[11] Malandrino A, Pozo JM, Castro-Mateos I, Frangi AF, van Rijsbergen MM, Ito K, et al. On the relative relevance of subject-specific geometries and degeneration-specific mechanical properties for the study of cell death in human intervertebral disk models. Front Bioengineer Biotechnol 2015;3:5.

[12] Rijsbergen MV, van Rietbergen B, Barthelemy V, et al. Comparison of patient-specific computational models vs. clinical follow-up, for adjacent segment disc degeneration and bone remodelling after spinal fusion. PLoS One 2018;13(8):e0200899.

[13] Castro-Mateos I, Pozo JM, Lazary A, Frangi A. 3D vertebra segmentation by feature selection active shape model. In: Yao J, Glocker B, Klinder T, Li S, editors. Recent advances in computational methods and clinical applications for spine imaging. Cham: Springer International Publishing; 2015. p. 241–5.

[14] Castro-Mateos I, Pozo JM, Eltes PE, Rio LD, Lazary A, Frangi AF. 3D segmentation of annulus fibrosus and nucleus pulposus from T2-weighted magnetic resonance images. Phys Med Biol 2014;59(24):7847–64.

[15] Cootes TF, Taylor CJ, Cooper DH, Graham J. Active shape models-their training and application. Comput Vision Image Understand 1995;61(1):38–59.

[16] Castro-Mateos I, Pozo JM, Lazary A, Frangi AF. Automatic construction of patient-specific finite-element mesh of the spine from IVDs and vertebra segmentations. In: Proceedings, Medical Imaging: Biomedical Applications in Molecular, Structural, and Functional Imaging, 9788; 2016..

[17] Horváth G, Koroknai G, Acs B, Than P, Illés T. Prevalence of low back pain and lumbar spine degenerative disorders. Questionnaire survey and clinical-radiological analysis of a representative Hungarian population. Int Orthop 2010;34(8):1245–9.

[18] Blanchard R, Morin C, Malandrino A, Vella A, Sant Z, Hellmich C. Patient-specific fracture risk assessment of vertebrae: a multiscale approach coupling x-ray physics and continuum micromechanics. Int J Numer Method Biomed Eng 2016;32(9):e02760.

[19] Schmidt H, Heuer F, Drumm J, Klezl Z, Claes L, Wilke HJ. Application of a calibration method provides more realistic results for a finite element model of a lumbar spinal segment. Clin Biomech 2007;22(4):377–84.

[20] Malandrino A, Lacroix D, Hellmich C, Ito K, Ferguson SJ, Noailly J. The role of endplate poromechanical properties on the nutrient availability in the intervertebral disc. Osteoarthr Cartil 2014;22(7):1053–60.

[21] Malandrino A, Noailly J, Lacroix D. Regional annulus fibre orientations used as a tool for the calibration of lumbar intervertebral disc finite element models. Comput Methods Biomech Biomed Eng 2013;16(9):923–8.

[22] Pfirrmann CW, Metzdorf A, Zanetti M, Hodler J, Boos N. Magnetic resonance classification of lumbar intervertebral disc degeneration. Spine 2001;26(17):1873–8.

[23] Noailly J, Ambrosio L, Elizabeth Tanner K, Planell JA, Lacroix D. In silico evaluation of a new composite disc substitute with a L3-L5 lumbar spine finite element model. Eur Spine J 2012;21(suppl 5):S675–87.

[24] Horn BKP. Closed-form solution of absolute orientation using unit quaternions. J Opt Soc Am A 1987;4(4):629–42.

[25] Kingma I, Busscher I, van der Veen AJ, Verkerke GJ, Veldhuizen AG, Homminga J, et al. Coupled motions in human and porcine thoracic and lumbar spines. J Biomech 2018;70:51–8.

[26] Kopperdahl DL, Keaveny TM. Yield strain behavior of trabecular bone. J Biomech 1998;31(7):601–8.

[27] Gawri R, Rosenzweig DH, Krock E, Ouellet JA, Stone LS, Quinn TM, et al. High mechanical strain of primary intervertebral disc cells promotes secretion of inflammatory factors associated with disc degeneration and pain. Arthritis Res Ther 2014;16(1). R21-R.

[28] Qian L, Jiang C, Sun P, Xu D, Wang Y, Fu M, et al. A comparison of the biomechanical stability of pedicle-lengthening screws and traditional pedicle screws. Bone Joint J 2018;100-B(4):516–21.

[29] Lorenz A, Leichtle CI, Frantz S, Bumann M, Tsiflikas I, Shiozawa T, et al. Pull out strength of dual outer diameter pedicle screws compared to uncemented and cemented standard pedicle screws: a biomechanical in vitro study. Orthop Surg 2017;9(2):229–36.

[30] Kwok AW, Finkelstein JA, Woodside T, Hearn TC, Hu RW. Insertional torque and pull-out strengths of conical and cylindrical pedicle screws in cadaveric bone. Spine 1996;21(21):2429–34.

[31] Panjabi MM, Oxland TR, Yamamoto I, Crisco JJ. Mechanical behavior of the human lumbar and lumbosacral spine as shown by three-dimensional load-displacement curves. J Bone Joint Surg Am Vol 1994;76(3):413–24.

[32] Oda I, Cunningham BW, Buckley RA, Goebel MJ, Haggerty CJ, Orbegoso CM, et al. Does spinal kyphotic deformity influence the biomechanical characteristics of the adjacent motion segments? An in vivo animal model. Spine 1999;24(20):2139–46.

[33] Heo Y, Park JH, Seong HY, Lee YS, Jeon SR, Rihm SC, et al. Symptomatic adjacent segment degeneration at the L3-4 level after fusion surgery at the L4-5 level: evaluation of the risk factors and 10-year incidence. Eur Spine J 2015;24(11):2474–80.

[34] Levangie PK, Norkin CC. Joint structure and function: a comprehensive analysis. Philadelphia, PA: F.A. Davis Co.; 2005.
[35] El-Bohy AA, Yang K-H, King AI. Experimental verification of facet load transmission by direct measurement of facet lamina contact pressure. J Biomech 1989;22(8):931–41.
[36] Du C-F, Yang N, Guo J-C, Huang Y-P, Zhang C. Biomechanical response of lumbar facet joints under follower preload: a finite element study. BMC Musculoskelet Disord 2016;17(1):126.
[37] Jaumard NV, Welch WC, Winkelstein BA. Spinal facet joint biomechanics and mechanotransduction in normal, injury and degenerative conditions. J Biomech Eng 2011;133(7):071010.
[38] Wang DL, Jiang SD, Dai LY. Biologic response of the intervertebral disc to static and dynamic compression in vitro. Spine 2007;32 (23):2521–8.
[39] Pattappa G, Li Z, Peroglio M, Wismer N, Alini M, Grad S. Diversity of intervertebral disc cells: phenotype and function. J Anat 2012;221 (6):480–96.
[40] Hadagali P, Peters JR, Balasubramanian S. Morphing the feature-based multi-blocks of normative/healthy vertebral geometries to scoliosis vertebral geometries: development of personalized finite element models. Comput Methods Biomech Biomed Eng 2018;21(4):297–324.
[41] Kumar MN, Jacquot F, Hall H. Long-term follow-up of functional outcomes and radiographic changes at adjacent levels following lumbar spine fusion for degenerative disc disease. Eur Spine J 2001;10 (4):309–13.
[42] Ghiselli G, Wang JC, Bhatia NN, Hsu WK, Dawson EG. Adjacent segment degeneration in the lumbar spine. J Bone Joint Surg Am Vol 2004;86(7):1497–503.
[43] Park P, Garton HJ, Gala VC, Hoff JT, McGillicuddy JE. Adjacent segment disease after lumbar or lumbosacral fusion: review of the literature. Spine 2004;29(17):1938–44.
[44] Radcliff KE, Kepler CK, Jakoi A, Sidhu GS, Rihn J, Vaccaro AR, et al. Adjacent segment disease in the lumbar spine following different treatment interventions. Spine J 2013;13(10):1339–49.
[45] Perez-Orribo L, Zucherman JF, Hsu KY, Reyes PM, Rodriguez-Martinez NG, Crawford NR. Biomechanics of a posterior lumbar motion stabilizing device: in vitro: comparison to intact and fused conditions. Spine 2016;41(2):E55–63.
[46] Hegewald AA, Hartmann S, Keiler A, Scheufler KM, Thomé C, Schmoelz W. Biomechanical investigation of lumbar hybrid stabilization in two-level posterior instrumentation. Eur Spine J 2018;27 (8):1887–94.